Group-level cortical surface parcellation with sulcal pits labeling

Irène Kaltenmark, Christine Deruelle, Lucile Brun,
Julien Lefèvre, Olivier Coulon, Guillaume Auzias

Contents

Abstract

Sulcal pits are the points of maximal depth within the folds of the cortical surface. These shape descriptors give a unique opportunity to access to a rich, fine-scale representation of the geometry and the developmental milestones of the cortical surface. However, using sulcal pits analysis at group level requires new numerical tools to establish inter-subject correspondences. Here, we address this issue by taking advantage of the geometrical information carried by sulcal basins that are the local patches of surfaces surrounding each sulcal pit. Our framework consists in two phases. First, we present a new method to generate a population-specific atlas of this sulcal basins organization as a fold-level parcellation of the cortical surface. Then, we address the labeling of individual sulcal pits and corresponding basins with respect to this atlas. To assess their validity, we applied these methodological advances on two different populations of healthy subjects. The first database of 137 adults allowed us to compare our method to the state-of-the-art and the second database of 209 children, aged between 0 and 18 years, illustrates the adaptability and relevance of our method in the context of pediatric data showing strong variations in cortical volume and folding.

1 Introduction

1.1 Context

The cortical surface presents an organization in folds that are highly variable in term of geometry and topology across individuals. The concept of sulcal roots emerged 20 years ago in Régis et al. (1995, 2005) as indivisible atomic folding entities located in the deeper parts of sulci corresponding to the location where the folding starts during the early phase of cortical development. In Lohmann and von Cramon (2000); Yang and Kruggel (2008); Li et al. (2009), the authors proposed a framework to decompose the folds of the cortical surface into several parcels called **sulcal basins** using a watershed approach. In order to give a concrete representation of the abstract concept of sulcal roots, Lohmann et al. (2008) introduced the **sulcal pits** as the deepest point of each sulcal basin.

A major interest of sulcal pits is to define a finite set of landmarks on the cortical surface allowing fine-scale comparison across individuals. A thorough review on sulcal pits studies has recently been presented in Im and Grant (2018). The sulcal pits have often been used to describe adult cortical morphometry (Im et al., 2010; Auzias et al., 2015; Takerkart et al., 2017; Le Guen et al., 2018) or atypical sulcal pattern in pathologies (Im et al., 2016). They are also of interest for tracking the growth and the evolution of the geometry of the cortical surface during brain maturation (Lefèvre et al., 2009; Kaltenmark et al., 2018). The longitudinal study of Meng et al. (2014, 2018) on the first two years of life highlighted a stable spatial distribution of pits in the major deepest folds already present at term birth. Authors also reported a regionally heterogeneous increase of sulcal pits depth, especially in the high-order association cortex. In Auzias et al. (2015), authors demonstrated that while deeper pits are less variable across subjects than superficial ones, some shallower sulcal pits also define robust landmarks of the cortical surface. The first study on young children covering both deep and shallow folds showed that the number of shallow pits increases with age between 18 months and 10 years (Brun et al., 2016).

Recently, Kruggel (2018) investigated the variability of the sulcal basins. He defined a subdivision of the neocortex minimizing the inter-individual variability. This approach led to an atlas of parcels, called communities, that are unions of sulcal basins and that are similar to the traditional concept of brain lobes. An atlas of sulcal basins consists in a further step to understand the sulcal organization of the cortical surface at finer scale. The statistical analysis of sulcal pits' properties relies on the **identification of homologous sulcal pits across subjects** that is made difficult by the large inter-subject variability. This task remains particularly challenging when working with sulcal pits covering the whole brain. The lack of methodological tools to address this issue prevents the fine-grained characterization of the spatio-temporal patterns of sulcal pits, in both deep and shallow folds.

1.2 Sulcal pits extraction with a watershed by flooding algorithm

Methods in the literature for computing the sulcal pits of an individual cortical surface rely on a **watershed by flooding algorithm on a smooth sulcal depth map** of the cortical surface. We briefly recall this algorithm. The vertices of the surface are ordered by their depth. The deepest vertex defines the first sulcal pit, the initial vertex of a sulcal basin. If the vertex next in the list is the neighbor of the previously identified sulcal basin, it is added to this sulcal basin. If all of its neighbors are unlabeled, it defines a new sulcal pit as a seed vertex for a new sulcal basin. This algorithm simulates water that would rise and fill the folds of the cortical surface with respect to the level sets of the depth map. By construction, the sulcal pits are the local maxima of this map.

Additionally, a merging procedure of the sulcal basins is applied during the watershed process to eliminate noisy pits that result from the spurious extrema related to anatomically irrelevant variations on the cortical surface (Lohmann and von Cramon, 2000; Rettmann et al., 2002; Im et al., 2010; Auzias et al., 2015).

1.3 Inter-subjects labeling of the sulcal pits

The latest methods to label sulcal pits across subjects (Im et al., 2010; Auzias et al., 2015) consist of a **registration of individual cortical surfaces** and a **clustering algorithm on the density map of sulcal pits** on the average surface. The spatial extent of the clusters is defined by application of a watershed on the density map. The labeling is then straightforward: each pit inherits the label of the cluster that contains it. In Im et al. (2010), if a subject has more than one pit present in a cluster, the authors used the distribution of sulcal pits in the cluster to select the pit that is closest to the densest point. In Auzias et al. (2015); Le Guen et al. (2018), the deepest pit is selected.

In Im et al. (2010), a depth threshold interrupts the watershed algorithm. The clusters only cover the deepest areas of the cortical surface and those located outside the deep major sulci are manually excluded. On the contrary, in Auzias et al. (2015), the authors run a complete watershed algorithm that segments the whole cortical surface in order to integrate the shallow pits in the labeling system and to avoid the manual selection of deeper folds. Between these two approaches, the number of group-level pit labels in the respective nomenclatures increased from 48 in the left and 47 in the right hemisphere in Im et al. (2010), to 104 and 114 respectively in Auzias et al. (2015). These numbers illustrate the tremendous increase in the complexity of inter-subjects labeling task when including shallower pits corresponding to more variable folds. However, the methodological advances presented in Auzias et al. (2015), focus on the optimization of sulcal pits extraction and not on the group-wise labeling. In the continuity of their work, the aim of this paper is to tackle this last task.

1.4 Methodological gap

In Kaltenmark et al. (2018), we observed an important number of outliers while analysing the sulcal pits spatial distribution. After thorough observation of individual data, we noticed that these outliers result from the lack of precision of the inter-individual labeling. At the same time, Le Guen et al. (2018) investigated the distribution of the sulcal pits depth in each cluster and they also highlighted the presence of outliers (despite the fact that they select for each subject the deepest pit in each cluster). They advocated that filtering these outliers was a difficult task that usually leads to the exclusion of true sulcal pits. They finally decided not to insert any thresholding step prior to their statistical analysis in order to preserve the largest sample possible representative from their data. **This noise induced by labeling errors, in data sets that already suffers from large inter-individual variability, is thus an important limitation to any statistical analysis.**

In this paper, we aim to address the following issues related to the inter-individual labeling task:

1. If a subject has more than one pit present in a cluster, there is no consensus on the automatic selection of the unique pit associated to the cluster.

2. Due to the spatial inter-individual variability, sulcal pits can be located at the boundary of some clusters, in which case their labeling is often unreliable.

3. Despite the important efforts of the community on the sulcal pits extraction procedure, some highly robust sulcal pits are missing in some subjects. As the respective clusters may be large, these subjects often do have a shallow pit in the area that is wrongly identified as the deep missing pit.

4. Regarding more specifically the group-wise watershed (see 1.3), the optimization of its parameters on a heterogeneous pediatric database has proven to be difficult and has not been investigated in the literature. No matter the choice of parameters, we always obtain a small number of clusters with a low pits frequency, which prevents to use this criterion to evaluate the parameters.

5. There is no ground truth established by medical experts in the literature to compare and to evaluate a labeling method of the sulcal pits (especially including the shallow pits). There are neither no methodological tools other than the frequency of sulcal pits in each cluster.

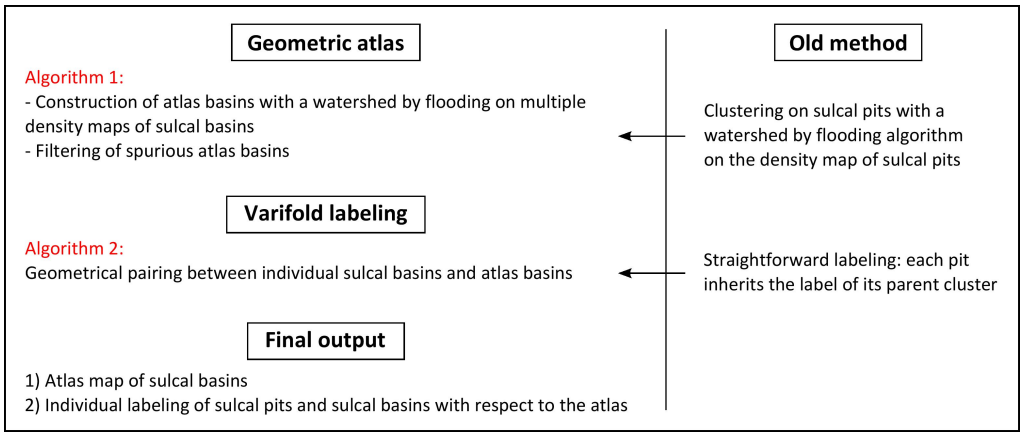

Figure 1: Overview of the complete pipeline referring to Algorithm 1 and Algorithm 2 of the Section Methods.

1.5 Contributions

We recall that the sulcal organization of individual cortical surfaces consists of a parcellation in sulcal basins with a unique sulcal pit in each basin (see 1.1). The most natural way to manually label a sulcal pit is to identify the part of the sulcus where the pit is located. This means to observe the local and geometric environment of the sulcal pit. Under the assumption that homologous sulcal pits across subjects are contained in similar sulcal basins, the approach developed in this paper consists in the analysis and labeling of **sulcal basins** to induce a labeling on the sulcal pits. We introduce a new pipeline composed of two phases. In Section 2, we first present a new method to generate a population-specific atlas of these sulcal basins under the form of a complete parcellation of a template cortical surface. We then address, in Section 3, the labeling of individual sulcal basins and corresponding pits with respect to the atlas. We keep the setup of registering every individual cortical surfaces on an average mesh (with FreeSurfer) and the challenging approach of considering both deep and shallow pits.

Unlike pits clusters, each region of our group-wise parcellation integrates the geometry of homologous individual sulcal basins. This means that their boundary tends to be aligned on

average with the boundary of the individual sulcal basins. We thus call these regions **atlas basins**. They replace the previous clusters of sulcal pits. They are the support of the second process that consists in comparisons and pairings between atlas basins and individual sulcal basins, with a similarity measure on surfaces. In the experiments, we use a measure induced by varifold metrics that are highly efficient as they are invariant to the parametrization of surfaces. Figure 1 gives an overview of the pipeline.

The lack of exact one-to-one correspondences across subjects is one of the main difficulties regarding the labeling task of sulcal basins and sulcal pits. For this reason, we introduce in the labeling system the concept of unlabeled sulcal pit, called **isolated pits**, in order to guarantee for each subject the **uniqueness of the sulcal pit identified by a label**. These isolated pits are the sulcal pits that cannot be identified by the atlas as they are not reproducible enough across the population.

The pipeline is applied to two different populations of healthy subjects. The first database consists of 137 adults from the Open Access Series of Imaging Studies (OASIS) database to show the improvement compared to previous approach of Auzias et al. (2015) and the application to a second population of 209 children, from the Cincinnati MR Imaging of Neurodevelopment (C-MIND) project, demonstrates the efficiency of the approach in a different context. Results are presented in Section 4 and discussed in Section 5.

In this work, we highlight the robustness of the sulcal basins through density maps of homologous sulcal basins, called **influence maps**. These maps also define a new qualitative measure to evaluate the generated atlas.

2 Methods. Part 1 : geometric atlas

This section presents the first algorithm of the pipeline: Algorithm 1. The central idea is to take into account the shape of individual sulcal basins to generate a group-wise parcellation of atlas basins on an average mesh. These atlas basins will locally play the role of geometric representatives of individual sulcal basins in terms of location and area.

Section 2.1 describes the initialization of the atlas basins. Section 2.2 introduces how we associate individual sulcal basins to atlas basins and how we extract their average shape through local density maps. Section 2.3 presents a new watershed by flooding process that provides a complete parcellation of atlas basins and Section 2.4 details the final step to remove noisy atlas basins.

Notation

Throughout this paper, we will denote B_k^A the k-th atlas basin of the atlas map. Given a population, we will denote p_j^i and B_j^i the j-th sulcal pit and the j-th sulcal basin of the i-th subject **after registration to the atlas mesh**. They are related by the relation $p_j^i \in B_j^i$. Finally, $x \in X$ will denote a vertex of the average cortical mesh. We will say that x is unlabeled if it does not belong to any atlas basin. The parcellation is complete when all vertices are labeled.

2.1 Initialization: seeds of the atlas basins

Given a set of cortical surfaces registered to a common template and their associated sulcal pits, a density map of sulcal pits was computed using the procedure of Auzias et al. (2015). The projection of smoothed individual sulcal pits on the template mesh were summed across subjects and normalized by the number of subjects. The maxima of this density map show the most robust locations of the pits at the population level. Vertices with locally maximal density were extracted and called **seeds of the atlas basins**. For each seed s_k, we initialized a new atlas basin B_k^A (to read k-th Atlas Basin) with the vertex of the seed.

2.2 Influence maps

For any atlas basin B_k^A, the sulcal pits located on the seed s_k initialize a list, denoted $Subj_k$, of homologous individual sulcal basins. More precisely, if p_j^i is on the seed s_k, then $(i,j) \in Subj_k$ and we say that B_j^i is **associated** to B_k^A. $Subj_k$ then defines the **influence map**, denoted I_k, of the atlas basin B_k^A. I_k is the local **density map of the sulcal basins associated to** B_k^A. For any vertex x, $I_k(x)$ is the percentage of sulcal basins associated to B_k^A that contains x :

$$I_k(x) = \frac{100}{\#Subj_k} \sum_{(i,j)\in Subj_k} \mathbb{1}_{B_j^i}(x)\,, \tag{1}$$

where $\#Subj_k$ is the number of pairs (i,j) in $Subj_k$, i.e. the number of associated basins, and $\mathbb{1}_{B_j^i}$ is the indicator function of the basin B_j^i.

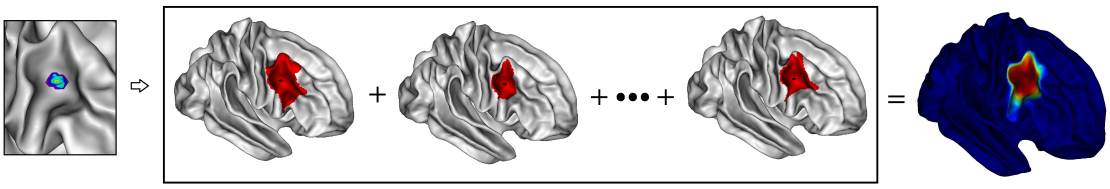

Figure 2: From left to right: Concentration of sulcal pits in an initial atlas basin. Extraction of individual sulcal basins associated to the atlas basin's pits. Influence map of the atlas basin.

Fig. 2 illustrates the construction of an influence map. Such map integrates the average location and shape of homologous sulcal basins. The level sets $\{I_k \geq \alpha\}$ are nested sets when α decreases from 100% to 0. In order to retrieve the shape of its associated basins, the atlas basin B_k^A will gradually grow by filling these nested sets until it reaches the boundaries of other atlas basins. Since we have as many influence maps as atlas basins, we cannot apply the standard watershed by flooding algorithm.

2.3 Adaptive watershed function

The adaptive watershed function is the core of Algorithm 1. This function segments the whole average mesh into atlas basins by iterating the three following steps:

1. For each unlabeled vertex $x \in X$, we identify the atlas basin $B_{k_x}^A$ with the maximal influence on x:

$$k_x = \arg\max_k I_k(x)\,, \tag{2}$$

   where k indexes the atlas basins. This defines for each vertex a unique attractive atlas basin.

2. We then extract an unlabeled vertex $\hat{x}$ whose attractive atlas basin has the maximal influence:

$$\hat{x} = \arg\max_x \mathrm{I}_{k_x}(x)\,, \tag{3}$$

3. $\hat{x}$ is added to its attractive atlas basin.

Remark 2.1. *The definition of the influence maps includes a normalization by the cardinal of $Subj_k$ in order to balance the atlas basins with spatially robust sulcal pits and the atlas basins with a lower peak of pits density. Otherwise, the first type of atlas basins would have higher influence and they would overextend at the expense of the second type.*

Another key element of our watershed function is to additionally identify new homologous individual basins, as the segmentation progresses. The lists $(Subj_k)_k$ will thus be gradually enhanced and the influence maps will accordingly be updated using equation (1).

2.3.1 Learning process: updating of the influence maps

Consider x a new vertex added to an atlas basin $B^A_{k_x}$ and p^i_j a sulcal pit on x. B^i_j is the individual sulcal basin that contains p^i_j. If B^i_j is homologous with the sulcal basins already associated to $B^A_{k_x}$, then its shape should be exploited to improve the robustness of the influence map I_{k_x}. To assess this homology, (i, j) is added to $Subj_{k_x}$ if and only if it satisfies both following conditions: For each new vertex x added to an atlas basin $B^A_{k_x}$ (Step 6 of Algorithm 1), the list $Subj_{k_x}$ is updated as follows (Step 7). For any sulcal pit p^i_j on x,

1. subject i is not already indexed by $Subj_{k_x}$,
2. the sulcal basin B^i_j contains the seed of the atlas basin $B^A_{k_x}$.

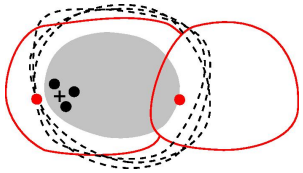

Figure 3: Illustration of the geometric criterion. We display the individual sulcal basins (black dashed lines) and the respective sulcal pits (black dots) of few subjects associated to a growing atlas basin (grey area). The seed of the atlas basin is marked by a +. Assume that the vertex with the right red pit has be assigned to the atlas basin. Due to the geometric criterion, the sulcal basin of this pit cannot be associated to the atlas basin. This prevents the atlas basin to overextend on the right side. It may however retrieve the left red pit and its basin at a later stage of the algorithm.

The first condition prevents two sulcal pits of the same subject to be associated to the same atlas basin (**uniqueness condition**). The second condition ensures that all the individual basins associated to an atlas basin are located around its seed (**geometrical criterion**). See Fig. 3 for schematic illustration. Fig. 4 illustrates the growth of an atlas basin and the update of its associated sulcal pits and sulcal basins on real data.

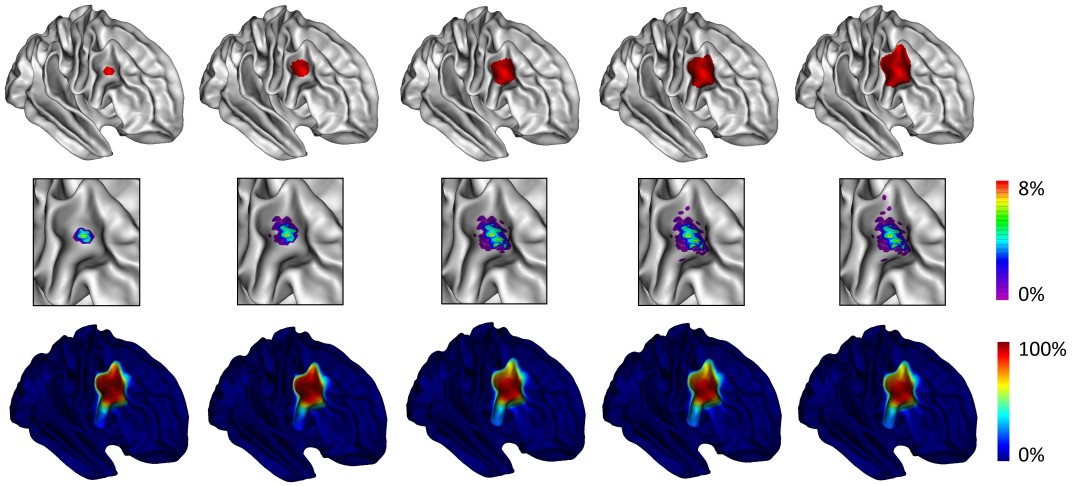

Figure 4: Growth of an atlas basin during the adaptive watershed algorithm. Second row: Pits' concentration. Third row: Influence map of the atlas basin.

Remark 2.2. *We call* ***isolated pits*** *the sulcal pits rejected by one of the two conditions. They can be individual noisy pits or part of a minor local pattern in the population, e.g. a region with*

two pits instead of one or a shallow pit on a gyrus. At this stage, these two conditions have not a huge impact but they will play ***a key role in the basin filtering procedure*** *in Section 2.4.2, as well as the isolated pits.*

2.3.2 Conflict of influence

Eq. (3) usually has multiple solutions. We define here a simple priority order to label a vertex among these solutions. Due to the spatial variability of the sulcal basins across individuals, the influence maps are smooth and their support overlap. This phenomenon highlights the uncertainty of the boundary of these atlas basins. Therefore, we propose to first label the vertex the most distant to these areas of uncertainty. This can be estimated by the notion of conflict.

Consider $x \in X$ and $B^A_{k_x}$ the atlas basin with the maximal influence on x. The conflict of influence with $B^A_{k_x}$ results from the influence of other basins and is defined by

$$C_{k_x}(x) = \sum_{k \neq k_x} I_k(x)^2 \,. \tag{4}$$

The conflict is high when x is close to at least one other atlas basin. Hence, between two vertices under maximal influence (i.e. solutions of eq. (3)), **we will first label the vertex with the lowest conflict** (Algorithm 1 Step 5). This reinforcement of the priority order in the iterative labeling of the vertices is numerically straightforward and it increases the benefit of the learning process of the algorithm.

2.4 Basin filtering

Due to the large inter-subject variability, which remains present even after surface registration, the density map of sulcal pits is irregular. As a consequence, it contains a lot of spurious maxima and our algorithm is initialized with a number of seeds much larger than the average number of sulcal pits. Referring to (Auzias et al., 2015), we chose to estimate the density map with a soft smoothing of the pits distribution to avoid the underestimation of these seeds and we developed an a posteriori strategy to filter the atlas basins. In the next sections, we detail how to delete an atlas basin and we then present a procedure to select and delete expendable atlas basins.

2.4.1 Atlas basin deletion

In the literature, the filtering of atlas basins is achieved by a straightforward merging between neighboring basins. This solution is yet not always the most pertinent one. In some situations, we would rather split a spurious atlas basin between several neighbors. Our adaptive watershed algorithm offers this flexibility. In order to delete an atlas basin $B^A_{k_D}$, we reset all the atlas basins to their respective seed. We then restart the **Adaptive watershed function** of Section 2.3 (or see Algorithm 1) to the new set of seeds after excluding the seed s_{k_D}.

When applying again this function, consider x a vertex that previously belonged to $B^A_{k_D}$. When the function estimates its attractive atlas basin (see equation (2)), **the influence map I_{k_D} does no longer exist** and x is thus attracted to a new atlas basin.

2.4.2 Atlas basin selection

Assume that we deleted a given atlas basin. The neighboring atlas basins have covered the region of the deleted basin and they eventually absorbed the sulcal pits in this region. Consider then the two opposite situations:

1. Most of the sulcal pits associated to the deleted basin have been associated to the neighboring atlas basins.

2. Due to the **uniqueness and geometric criteria**, the neighboring basins were not allowed to inherit these new pits. These pits became isolated pits (see Remark 2.2).

The first situation confirms that the deleted basin was a spurious basin. In the second case, the basin represented a pattern of sulcal features (pits and basins) that we may want to preserve.

The choice of the atlas basin to delete should thus aim at minimizing the number of lost pits after a deletion, i.e. the number of additional isolated pits. In practice, this is equivalent to maximizing the total number of labeled pits after a deletion. With the notation of Auzias et al. (2015), for any atlas basin B_k^A, $N_1(k)$ is the percentage of subjects that have one (and only one) sulcal pit associated to B_k^A. In the **Basin filtering** function of Algorithm 1, we will estimate the total number of labeled pits for every single atlas basin deletion possible and select *a posteriori* the optimal atlas basin to delete. The deletion simulations are achieved in Step (1) and the optimal configuration is identified in Step (2).

Finally, we define the following stop criterion. The atlas basin deletion stops when the minimal N_1 score of the current atlas basins is above a given threshold p. The algorithm stops when each atlas basin has a percentage of homologous individual basins across the population greater than p. This threshold defines the flexibility with respect to minor patterns of sulcal pits that we want to integrate in the atlas.

3 Methods. Part 2 : individual pits labeling with varifold comparison

In Section 2, we presented a new automatic method to create an atlas parcellation from a population of individual cortical parcellations. Each region of this atlas, called atlas basin, integrates the average geometry of homologous individual sulcal basins across the population. We can now exploit these geometric similarities in order to optimally identify the representative atlas basin of each individual sulcal basin. We compare individual sulcal basins to atlas basins with a similarity measure $\mathcal{M}$ on surfaces. The optimal pairing of these entities will induce the labeling of the sulcal pits. We used an oriented varifold metric which compares the positions, areas, and orientations of the surfaces Charon and Trouvé (2013); Kaltenmark et al. (2017). The varifold representation does not depend on the shape parametrization which allows to compare surfaces with a different number of vertices. The family of metrics on currents, varifolds and oriented varifolds are increasingly being used in a complex setting of shape registration by large deformations. We illustrate here how these metrics can be used outside this setting as simple similarity measures like a Dice index but more precise.

Given a registered subject, the identification with the atlas is achieved in two steps presented in Algorithm 2. **Step 2** is the core of the algorithm: we estimate for each atlas basin the best geometric match among the individual sulcal basins with respect to the similarity measure $\mathcal{M}$. In order to define a unique label to the individual sulcal basin, once a subject basin is paired to an atlas basin, it can no longer be candidate for a new match. As the number of pits varies across individuals, we do not expect to retrieve a one-to-one correspondence between individual and atlas basins. This means that when an atlas basin has no anatomical homologous subject basin, its best geometric match is irrelevant. To prevent undesirable pairings, our strategy relies on two properties:

- Given a best candidate for an atlas basin, we verify that this candidate is sound with a straightforward condition that we can easily interpret. Denote $\mathcal{A}$ the function that returns the area of a surface. The pairing between an atlas basin and the best subject basin is validated if their overlap is large enough. This condition is formalized by inequalities of the type $\mathcal{A}(B \cap \overline{B}) > P\%\mathcal{A}(\overline{B})$ meaning that the intersection of two basins B and $\overline{B}$ fills at least $P\%$ of $\overline{B}$, with P a given threshold.

- The most reproducible atlas basins should more likely find a match than the others. Therefore, atlas basins are ordered in a list denoted $\overline{Q}$ by decreasing robustness. Each atlas basin of this list is compared to all the unmatched subject basins in order to find the best candidate. The robustness of atlas basins is estimated by the maximal sulcal pits density in each atlas basins.

Algorithm 1: Adaptive watershed algorithm

Initialization:

- Extract the seeds, which are the maxima of the density map.
- Initialize the atlas basins by the 2-ring neighborhood of the seeds.
- Initialize the respective lists $Subj_k$.

Adaptive watershed function:

1. If all the vertices are labeled, the atlas is complete. Otherwise:
2. Using the lists $(Subj_k)_k$, compute the influence map of each atlas basin.
3. Restrict each influence map to the unlabeled vertices at the boundary of their respective atlas basin.
4. Extract the vertices under maximal influence:
$$\arg\max_x \max_k I_k(x)$$
5. Select among them a vertex x with minimal conflict.
6. x inherits the label k_x where k_x indexes the atlas basin with maximal influence on x. $B^A_{k_x} \leftarrow B^A_{k_x} \cup \{x\}$.
7. Update $Subj_{k_x}$: pits on the vertex x are associated to the atlas basin $B^A_{k_x}$.
8. Return to Step (1).

Basin filtering:

Compute N_1.

While $\min_{k\in[1:n]} N_1(k) < p$, do:

1. **For** $k_0 \in [1:n]$, do:
i) Simulate the deletion of the atlas basin $B_A(k_0)$.
ii) Compute the temporary N_1 score, denoted $N_1^{k_0}$, associated to the resulting parcellation without the atlas basin $B_A(k_0)$.
iii) Compute $Tot(k_0) = \sum_{k\in[1:n],k\neq k_0} N_1^{k_0}(k)$.
2. Select $k_D = \arg\max_{k\in[1:n]} Tot(k)$.
3. Delete definitively the atlas basin $B^A_{k_D}$.
4. Re-index the remaining atlas basins:
$$n \leftarrow n-1,\ N_1 \leftarrow N_1^{k_D}.$$

This approach relies on the reproducibility of the sulcal basins. Observation of the data showed that this well-founded hypothesis is yet patently not satisfied in one marginal situation: a subject misses pits in a cortical fold and this fold is represented by a unique large basin (see Fig. 6). This basin covers thus one or more atlas basins. Such large individual basins should not be compared to atlas basins as surfaces. We will therefore preprocess the identification of these basins. In Algorithm 2 **Step 1**, a small number of individual basins are associated to atlas basins according to the position of their sulcal pits. More precisely, for any individual sulcal basin B, we compare its area with the area of the atlas basin $\overline{B}$ that contains the sulcal pit of B. If $\mathcal{A}(B)$ is twice larger than $\mathcal{A}(\overline{B})$, B is considered as a large basin and its pit inherits the label of $\overline{B}$. For consistency reasons, the previous necessary condition on the overlap between two queried basins is also tested to validate any pairing.

Each labeled individual basin contains a unique sulcal pit that straightforwardly inherits the same label. A novelty of this approach, regarding the methods in the literature, is that a sulcal pit can be assigned to an atlas basin that does not contain it as illustrated in Fig. 5 (third example). However, the overlap criterion always ensures that this atlas basin does overlap subsequently with the pit's basin. Fig. 5 illustrates two other valid matchings and two rejected matchings.

At the end of Step 2, when all atlas basins have been queried for an optimal match, some individual sulcal basins remain unlabeled as well as their sulcal pits. By analogy with the method presented in Section 2, we call them again the **isolated pits** (see 2.2).

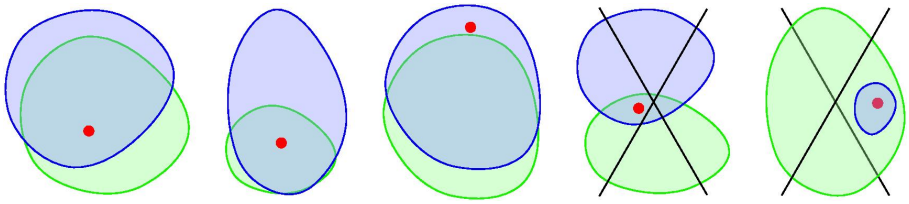

Figure 5: Attempts of matching between a subject basin and an atlas atlas basin. The third matching illustrates the flexibility of our method: the sulcal pit is outside its associated atlas basin.

Algorithm 2: Pits labeling with varifold comparison

Input : A subject given by its sulcal pits and sulcal basins registered on an atlas mesh. An atlas parcellation of this mesh in atlas basins.

Output: A set of pairings between the individual sulcal basins and the atlas basins.

Step 1: Order subject basins by decreasing area in a queue Q. For each basin $B \in Q$, consider the atlas basin $\overline{B}$ that contains the subject pit.
(a) If $\mathcal{A}(B \cap \overline{B}) > 80\%\mathcal{A}(\overline{B})$, the pit is assigned to $\overline{B}$ and $\overline{B}$ is removed of $\overline{Q}$.
(b) If the area of B is twice larger than the area of $\overline{B}$, and if $\mathcal{A}(B \cap \overline{B}) > 50\%\mathcal{A}(\overline{B})$, the pit is assigned to $\overline{B}$ and $\overline{B}$ is removed of $\overline{Q}$.

Step 2: For each atlas basin $\overline{B} \in \overline{Q}$, ordered unassigned subject basins in a new list Q' by decreasing distance to $\overline{B}$ with respect to the similarity measure $\mathcal{M}$. Select the first subject basin $B \in Q'$ that satisfies either $\mathcal{A}(B \cap \overline{B}) > 50\%\mathcal{A}(\overline{B})$ or $\mathcal{A}(B \cap \overline{B}) > 50\%\mathcal{A}(B)$.

Remark 3.1 (Algorithm details)**.** *The distance in Step 2 is the norm of the difference between two basins represented by oriented varifolds. This norm is induced by the following scalar product:*

$$\langle \mu_X, \mu_Y \rangle = \sum_{i=1}^{F^X} \sum_{j=1}^{F^Y} k_{pos}(x_i, y_j) k_{or}(\vec{t}_i^X, \vec{t}_j^Y) r_i^X r_j^Y \tag{5}$$

where X and Y are the triangulated meshes of two basins B and $\overline{B}$, μ_X and μ_Y are their respective varifold representation that is, e.g. for X, the distribution of the tangent vectors $\vec{t}_i^X$, on the center points $(x_i)_i$ of the F^X faces of X, and weighted by the areas $(r_i^X)_i$ of these faces. In the experiments, we will use two Gaussian kernels

$$k_{pos}(x,y) = e^{-\frac{|x-y|^2}{\sigma^2}}, \qquad k_{or}(\vec{t}_i,\vec{t}_j) = e^{\frac{2(\vec{t}_i\cdot\vec{t}_j)}{\sigma_s^2}}, \tag{6}$$

where the main scale parameter is set to $\sigma = 15mm$ and the other one, on the angular sensitivity, is set to $\sigma_s = 0.5$. We recall that all cortical surfaces are registered on an average mesh and that we compare the basins after registration. The scale parameter is adjusted to the size of this mesh (the length of each hemisphere is about 17cm).

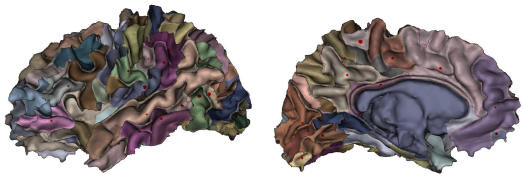

Figure 6: Example of a subject with an unusual large basin in the superior temporal sulcus (left panel) and two others in the frontal lobe (right panel).

4 Experiments and results

In order to evaluate our pipeline (summarized in Fig. 1), we first used the adult database studied in Auzias et al. (2015). We compare their results with ours. We will then present a second application to a pediatric database with a large range of ages. While these two populations are too different to run a robustness study, our pipeline applied with the same parameters results in anatomically relevant atlases and inter-subject labeling in both populations.

More precisely, we computed for each population and each hemisphere a specific atlas with the first part of our pipeline. We then labeled each subject according to their respective atlas with the varifold labeling method. This labeling will be evaluated at the group level through the N_1 score (the percentage of subjects that have a pit associated to the basin) and the density maps of homologous sulcal basins. We recall that subjects have no more than one sulcal pits associated to an atlas basin. Few sulcal pits remain unlabeled (the isolated pits).

4.1 Data acquisition and preprocessing

OASIS database: This data was used in Auzias et al. (2015) and consists in 137 right-handed young adult healthy subjects, aged from 18 to 34, selected from the Open Access Series of Imaging Studies (OASIS) database (www.oasis-brains.org) Marcus et al. (2007). For each subject, three to four individual T1-weighted magnetization prepared rapid gradient echo (MP-RAGE) scans were obtained on a 1.5 T Vision system (Siemens, Erlangen, Germany) with the following protocol: in-plane resolution = 256 × 256 (1 mm × 1 mm), slice thickness= 1.25 mm, TR= 9.7 ms, TE = 4 ms, flip angle = 10u, TI = 20 ms, TD = 200 ms. Images were motion corrected and averaged to create a single image with a high contrast-to-noise ratio Marcus et al. (2007). Anatomical MR images were processed using Freesurfer v5.1.0, in order to extract the inner cortical surface mesh, surface area, intracranial volume and obtain spherical interindividual correspondences Dale et al. (1999); Fischl (2012).

CMIND database: 155 healthy children, between 9 months and 18-years-old, were selected form the Cincinnati MR Imaging of Neurodevelopment (C-MIND) project (04/30/2015 release). Among them 55 subjects were scanned longitudinally with two or three timesteps. For each

timestep, one or two T1w images were acquired on a Philips 3T MRI scanner with the following protocol: matrix size = 256 × 224, spatial resolution = 1 mm × 1 mm × 1 mm, TR/TE = 8.1/3.7 ms, flip angle = 8°, TI = 939 ms. These images were denoised using SPM8 (SANLM algorithm) and a grey/white matter segmentation was performed using FreeSurfer 5.3.0. For 10 of these subjects, manual correction using the control points of FreeSurfer was applied.

The extraction of sulcal pits was performed using the procedure of Auzias et al. (2015), designed to yield reproducible sulcal pits especially in children populations (see Section 1.2). Correspondences between cortical meshes were then obtained by spherical alignment using Freesurfer Fischl (2012). We used a single average mesh estimated with the OASIS database (with 41000 vertices for each hemisphere). To remove the non-cortex part of this mesh (cingular mask), we summed all the individually registered cingular masks and we extracted the vertices that belong to more than 70% of the population. Each individual map showing the localization of the sulcal pits was then projected onto a template surface, after smoothing with an FWHM of 5 mm, maintaining a peak value of 1 Auzias et al. (2015). Note that the previous method was based on clustering the density map of sulcal pits. The level lines of this map strongly depends on the smoothing process of the sulcal pits. Our algorithm only extracts the extrema of this map. It is therefore significantly more robust to the smoothing parameters. Regarding the estimation of the sulcal depth, we used the Depth Potential Function (DPF), as in Auzias et al. (2015).

4.2 Algorithm details

In order to produce a more robust stop criterion in the basin filtering step of Algorithm 1, we considered the average N_1 score of the 5 less reproducible atlas basins instead of the minimal N_1. The threshold for this average is set to $p = 25\%$. The stop criterion of the while loop is:

$$\text{mean}(N_1(k_i))_{i=1..5} < p\,,$$

where for any $k \notin (k_i)_i, N_1(k) \geq \max_i N_1(k_i)$.

The basin filtering step of Algorithm 1 is numerically expensive as we simulate the deletion of **each** atlas basin at each iteration (factorial process with respect to the number of initial atlas basins). The first iterations are the most time-consuming since the atlas contains more basins than during the last iterations. Moreover, the irregularity of the density map of sulcal pits induces too many maxima that initialize the seeds of the atlas basins. This map provides between 200 and 250 seeds when subjects have about 100 sulcal pits. The following minor changes reduce the run-time from 4-5 days to 2-3 hours:

1. We start the Basin filtering function of Algorithm 1 by deleting the atlas basins with a N_1 score lower than 10%.

2. Then, in the first step of the while loop, we only consider the atlas basins with a N_1 score lower than 70% since we do not want to delete well filled atlas basins.

3. When simulating a basin's deletion in the for loop, we only reset the labels of the vertices in the atlas basin to remove (see Section 2.4.1). Once we have estimated the optimal configuration, i.e. the optimal atlas basin to delete, we reset all the vertices in Step (3) to compute the new atlas with the adaptive watershed function.

At the initialization of Algorithm 1, we have no warranty that each seed actually contains sulcal pits. The vertex could indeed be the barycenter of some pits in its close neighborhood. Without pits, the influence map of the atlas basin cannot be initialized, the basin cannot grow and it would be deleted at the filtering step. Therefore, we initialize each atlas basin to a 2-ring neighborhood of the seeds (average radius of 2.5mm, Fig 4 first row, first column illustrates the initial 2-ring neighborhood of a seed). This ensures to have enough sulcal pits to generate a robust first estimation of the influence maps of each atlas basin. Note that for almost all atlas basins, these vertices would have been identically labeled by the Adaptive watershed function. At last, at the individual level, sulcal pits are located in distinct sulcal basins and they are by construction well separated.

Table 1: OASIS: Number of atlas basins, number of labeled sulcal pits and comparison with the old pipeline.

		New pipeline		Auzias et al. (2015)	
Hemisphere	# Sulcal pits	# Atlas basins	% Labeled pits	# Pits clusters	% Labeled pits
Left	88.3 ± 4.7	92	82.3%	104	82.4%
Right	89.5 ± 5.1	90	81.4%	114	85.7%

Two atlas basins that are not disjoint at this stage contain thus homologous sulcal pits across the population. In this case, we delete the atlas basin with the lowest peak of pits density. This ensures that all atlas basins are disjoint before starting the watershed process (this is equivalent to say that we filter the seeds to ensure a minimal geodesic distance of 5mm).

Remark 4.1. *Note that the initial subjects of different seeds are not necessary the same. These subjects are locally chosen for an implicit similarity property of their sulcal basin at a specific location: the associated sulcal pits are at this specific location. Hence, the overall initialization is not based on few subjects. Then, Fig. 4 illustrates on row 2, how an atlas basin quickly takes into account additional subjects.*

Run-times on one hemisphere mesh of 41000 vertices for a population of 137 subjects (OASIS database) :

- Algorithm 1 : 2-3 hours.
- Algorithm 2 : The overlap criterion allows to only compute the varifold metric between admissible pairs of basins. We also added in Step 1 (a) the automatic labeling of individual sulcal basin that strongly overlap with the atlas basin containing the sulcal pit. *In fine*, Algorithm 2 runs for about 2 hours.

4.3 Results on OASIS

On average, subjects have 88.3 ± 4.7 sulcal pits on the left hemisphere and 89.5 ± 5.1 on the right hemisphere. We identified 92 atlas basins on the left hemisphere and 90 atlas basins on the right hemisphere. In Auzias et al. (2015), the atlas has instead 104 pits clusters on the left hemisphere and 114 on the right hemisphere. With their pipeline, a subject can have more than one sulcal pit in the same atlas basin. In order to compare the sulcal pit's labeling of the two pipelines, in case of multi-labeling with the method of Auzias et al. (2015), we selected, for any following analysis, the closest pit to the peak of pits' density in the cluster. The old pipeline labeled for each subject about 72.8 sulcal pits on the left hemisphere and 76.7 on the right hemisphere, i.e. 82.4% and 85.7% of the pits. The new pipeline labeled respectively 72.7 and 72.9 sulcal pits, i.e. 82.3% and 81.4% of the pits. Despite the large reduction of the number of atlas basins, the identification of the sulcal pits is thus quantitatively similar (with 24 additional clusters, the old pipeline only labels 4 additional sulcal pits on the right hemisphere). See Tab. 1.

The percentages of sulcal pits associated to each atlas basin across the population, i.e. the N_1 scores, are reported in Tab. 2 and displayed in Fig. 10 (a), rows 1 and 2. In overall, we retrieved mostly the same basins than Auzias et al. (2015) but most clusters with a low N_1 score no longer appear (blue basins). In order to make a fair comparison of the N_1 scores on the most reliable atlas basins, we excluded the less reproducible clusters of the old method. For the sake of simplicity, we aligned the number of atlas basins of each method, i.e. we selected for the old pipeline the 92 and 90 best N_1 scores on the left and right hemispheres. We then computed the average N_1 scores of the two methods. Despite this selection, the new pipeline still presents the best scores and with a smaller variance.

The specificity of our method is to generate atlas basins that are geometrically good representatives of the individual sulcal basins. Regarding this goal, we can observe that the boundaries of

Table 2: OASIS: Average N_1 score.

	New pipeline	Auzias et al. (2015)	
Hemisphere	Average N_1	Filtered average N_1	# Excluded clusters
Left	79.0 ± 17.4 %	76.8 ± 21.8 %	12
Right	81.0 ± 18.0 %	78.3 ± 18.6 %	24

our atlas basins are very well aligned with the geometry of the atlas mesh which suggests that we indeed retrieved the average boundaries of sulcal basins. Conversely, purple arrows in Fig. 10 (a) highlight clusters of the old pipeline that cover gyri. Typically, the boundary of these clusters is not aligned with the crest line. These clusters overflows into their adjacent sulci.

4.4 Results on CMIND

Table 3: CMIND: Number of atlas basins, number of labeled sulcal pits and average N_1 score.

Hemisphere	# Sulcal pits	# Atlas basins	% Labeled pits	Average N_1
Left	97 ± 6.9	103	82.9%	78.0 ± 18.1 %
Right	99.2 ± 6.8	99	80.4%	80.6 ± 16.8 %

This database presents 97 ± 6.9 sulcal pits by subject on the left hemisphere and 99.2 ± 6.8 on the right hemisphere. We identified 100 atlas basins on the left hemisphere and 102 atlas basins on the right hemisphere. Regarding the labeling, in average, our pipeline identified for each subject 82.9% of the sulcal pits on the left hemisphere and 80.4% on the right hemisphere. The average N_1 score is 78.0 ± 18.1 % on the left hemisphere and 80.6 ± 16.8 % on the right hemisphere. See Tab. 3. The N_1 scores of the atlas basins are presented in Fig. 10 (b). As for the adult database, only few atlas basins have a low N_1 (light blue).

In Fig. 7, we display the resulting labeling on three subjects and we pullback the labeling on their original cortical surfaces. We selected the youngest, the median and the oldest subject of the CMIND population (resp. 1, 9, 18 years old). In the superior temporal sulcus (STS), the brown and dark purple basins are not present in the first subject. Conversely, the second subject has an additional white basin in the STS that does not exist in the atlas. The white color corresponds to the unlabeled pits, i.e. the isolated pits. Likewise, the last subject has an additional white basin in the central sulcus.

4.5 Atlas asymmetries

We presented in (Auzias et al., 2015) a procedure to investigate properly the asymmetries in sulcal pits distribution and characteristics. As detailed in that paper, inter-hemispheric registration and atlas construction from both hemispheres are required to enable quantitative analysis of asymmetries. We did not achieve these processing steps in the current work since the focus here is on the atlas basins definition and inter-subjects labeling. Qualitatively, the comparison across hemispheres of the shape and N_1 maps from Fig. 10 suggests that a quantitative analysis as done in (Auzias et al., 2015) on pits frequency would give similar results, with most marked asymmetries located in the temporo-parietal region and posterior part of the Sylvian fissure, as well as in the post-central region. The presence of an additional basin in the superior temporal sulcus of left hemisphere compared to right is consistent with previous observation in (Auzias et al., 2015). This asymmetry in this language-related region is observed in both OASIS and CMIND populations.

In the next sections, we introduce a new tool to validate the labeling.

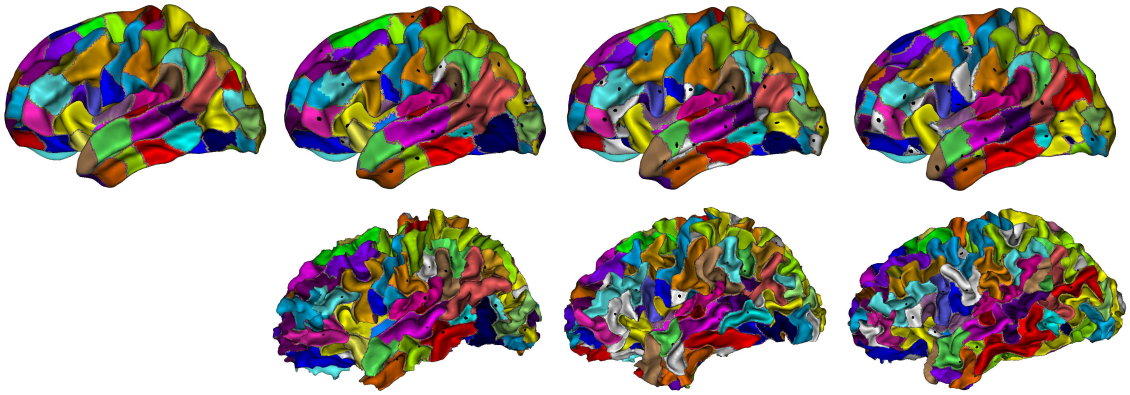

Figure 7: (CMIND) Atlas basins and three examples of individual labeling on the left hemisphere (on template on top, original surface on the bottom). The subjects are respectively the youngest, the median and the oldest of the population. The white color corresponds to the unlabeled pits, i.e. the isolated pits.

4.6 Atlas and labeling evaluations: local example

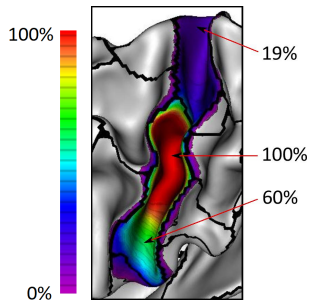

Figure 8: (OASIS) Density map of the individual sulcal basins for the label corresponding to the middle atlas basin of the central sulcus.

Let us recall that for any atlas basin, its influence map is the density map of its associated individual sulcal basins. In order to evaluate our complete pipeline, we computed these maps with respect to the labeling of the varifold method presented in Section 3. Fig. 8 presents the influence map of the central atlas basin in the central sulcus (CS) in the OASIS population. The large red area corresponds to a density of 100%. This means that **all the vertices in this area belong to every individual basins under this label**. Moreover, the frequency of this atlas basin is 100% (see Fig. 10). This shows that **we correctly identified the central basin of the CS for every subject of the OASIS population**. This large intersection highlights the important stability of this basin. However, this map also contains a lot of information on minor patterns of variability:

- The dark purple area on the top of the sulcus indicates that 19% of individual sulcal basins are extended up to the top of the sulcus which also means that their subject do not have an additional sulcal pit in this area. Note that this pattern is not clearly apparent in the pattern analysis of neonatal brains of Meng et al. (2018) (see Fig. 3).
- Regarding the discontinuous jump of density between the red area and the dark purple area, we deduce that **81% of the subjects have a clean and highly reproducible top boundary of their central sulcal basin at the location of the hand knob**.

- Conversely, the numerous level lines at the bottom of the central sulcus indicate a continuous variability of the bottom boundary of the individual sulcal basins.

In conclusion, the influence maps introduced in this paper are a very powerful tool to validate locally the labeling and to analyze the geometry of sulcal basins at the group level. Such detailed analysis of each influence map goes beyond the scope of this paper. However, we present in the next section a global analysis of these maps.

4.7 Atlas and labeling evaluations: global analysis

In order to visualize all the influence maps (at least partially), we display on a single mesh in Fig. 10 the restriction of each map to its respective atlas basin. With the new pipeline, most of the atlas basins are significantly filled in red which indicates a dense and large overlap in each group of homologous sulcal basins. A small and sharp decrease of the density at proximity of the boundaries shows that individual boundaries are well aligned (thin yellow auras on the boundaries of each atlas basins). In conclusion, **the atlas basins are geometrically good representatives of the individual basins and the labeling is globally consistent**. Few blue-green areas highlight regions where a minority of subjects present a different basin pattern. Most likely these subjects share an additional sulcal basin in these areas. We recall at last that these influence maps are normalized. Consequently, some atlas basins may have a low N_1 score and a high influence map. This means that they are good representatives of the subset of the population that have a basin at this place. Let us note that the notion of variability maps introduced in Kruggel (2018) is in the same spirit that our fusion of density maps and could also be investigated to evaluate the quality of an atlas.

Likewise, we computed the influence maps associated to the clusters and the labeling of Auzias et al. (2015) (see Fig. 10, third row). The first observation is that pits clusters do not match the average shapes of homologous sulcal basins. The numerous clusters with dark blue areas are too large with respect to the individual basins, which we already noticed through the misalignment of the boundaries with the geometry of the average mesh (see the purple arrows). Regarding the labeling, the peaks of density in each cluster is in overall significantly smaller than with our method (see e.g. in the frontal lobe). This means that the overlap between homologous sulcal basins is less important which shows that the old pipeline provides less robust sets of homologous sulcal basins. In particular, some clusters with a high N_1 score, reach a peak around 60% (yellow clusters). This means that the pipeline was not able to exclude isolated pits or it mixed multimodal distribution of sulcal pits.

Remark 4.2. *To illustrate again how to read these influence maps, we denoted two clusters in the superior temporal sulcus (Fig. 10 a) arrows 1 and 2). The density in cluster 2 remains very high on the left boundary. This indicates that most of the associated basins overextend the cluster to the left. This is also confirmed by the low density in cluster 1 on its right boundary. Most of the associated basins do not reach this boundary that should be slightly shifted towards the left as it is corrected in our new atlas. The misplacement of this boundary induces labeling errors. Indeed, the N_1 score of cluster 2 is smaller than its equivalent atlas basin in the new atlas: 92% against 98%. Yet, the maximal density of its influence map is also smaller 90% against 95%. This means that we captured more basins and better aligned in this area.*

To go further on the comparison of the two methods, we investigated the depth of sulcal pits, estimated with the depth potential map. Fig. 9 shows for each pipeline the average depth in *deep* atlas basins. The new atlas tends more to the blue and is more homogeneous. More generally, Fig. 9 also displays the standard deviation (STD) of the sulcal pits' depth. With the exception of shallowest basins where the variability can result from a large set of factors, the STD is globally smaller with the new atlas. **These observations and the previous analysis of the influence maps establish the improvement of our labeling method.**

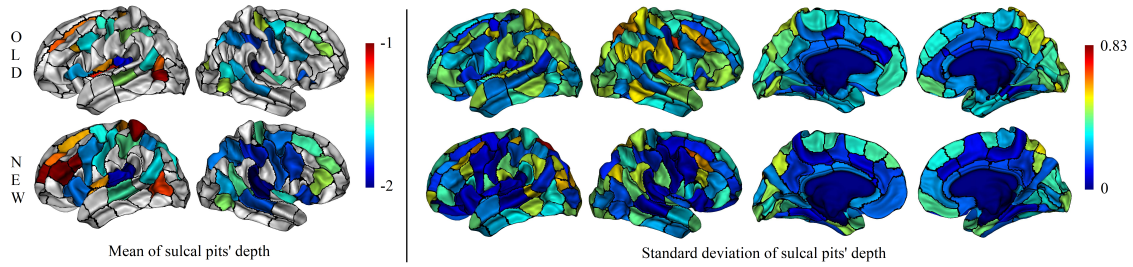

Figure 9: (OASIS) Left: Mean of sulcal pits' depth of the deepest atlas basins (resp. clusters) (with a threshold at -1). Note that, on the whole cortical surface, the depth potential map (DPF) takes values between -2 and 0.3 with negative values for the deepest points. Right: Standard deviation of sulcal pits' depth for each atlas basin (resp. cluster). Old pipeline (first row) and new pipeline (second row).

5 Discussion

Auzias et al. (2015) is the first work that integrated shallow pits in the analysis of the sulcal organization of the brain. However, the paper focuses on the extraction of sulcal pits on individual surfaces. In the continuity of their work, our method addresses the labeling task of sulcal basins. Fig. 7 illustrates the complexity of this task compared to the labeling of sulci. The construction of geometric population-specific atlases of sulcal basins is a first step to better understand this fine-scale organization of the cortical surface.

The evaluation of our pipeline is difficult as there is no gold standard nomenclature of sulcal basins (especially including shallow folds), which thus excludes a straightforward automatic validation of the labeling. In this context, we first relied on the pits frequency of each basin at the group level, i.e. the N_1 score reported above, to get a first quantitative evaluation of the labeling results. However, our approach offers a new powerful tool to address the validation of such methods: the density map associated with each atlas basin provides a quantitative and qualitative measure of how well the basin matches the population.

We presented Section 2.4 an original method to filter spurious atlas basins. In previous methods based on a watershed by flooding algorithm applied to the pits density map, the merging decision of two atlas basins was driven by three geometric properties (basins area, ridge height and geodesic distance). However, the associated threshold parameters are difficult to adjust for different populations. They depend on pits location and frequency, as well as the amount of smoothing applied to regularize the density map. The influence of each parameter of the watershed is thus very difficult to interpret and is locally variable. In particular, the ridge height between two basins depends on the local pattern, such that two neighboring basins can be merged if they are spatially too close even if their respective density peaks are high. Our strategy is strongly different: an atlas basin is preserved if the algorithm found more than $p\%$ homologous sulcal basins among the population (see Section 2.4.2). The filtering decision is reduced to a single parameter. The interpretation of this parameter is simpler since its influence is global and not local. As an illustration, we used in the experiments the same parameter $p = 25\%$ for two different populations (OASIS and CMIND) and both hemispheres. In these four cases, we observed a similar percentage of labeled pits (between 80.4% and 82.9%) combined with a good N_1 score (between 78.0% and 81.0%). Moreover, the influence maps validated the pipeline on a more qualitative level (see Section 4.7). This consistency across different datasets and hemispheres underlie the stability of the proposed framework.

5.1 Atlas: uniqueness

The construction of an atlas of sulcal basins is the first step to understand the sulcal organization of the cortical surface at this fine scale. Cortical variability is not spatially uniform and the notion

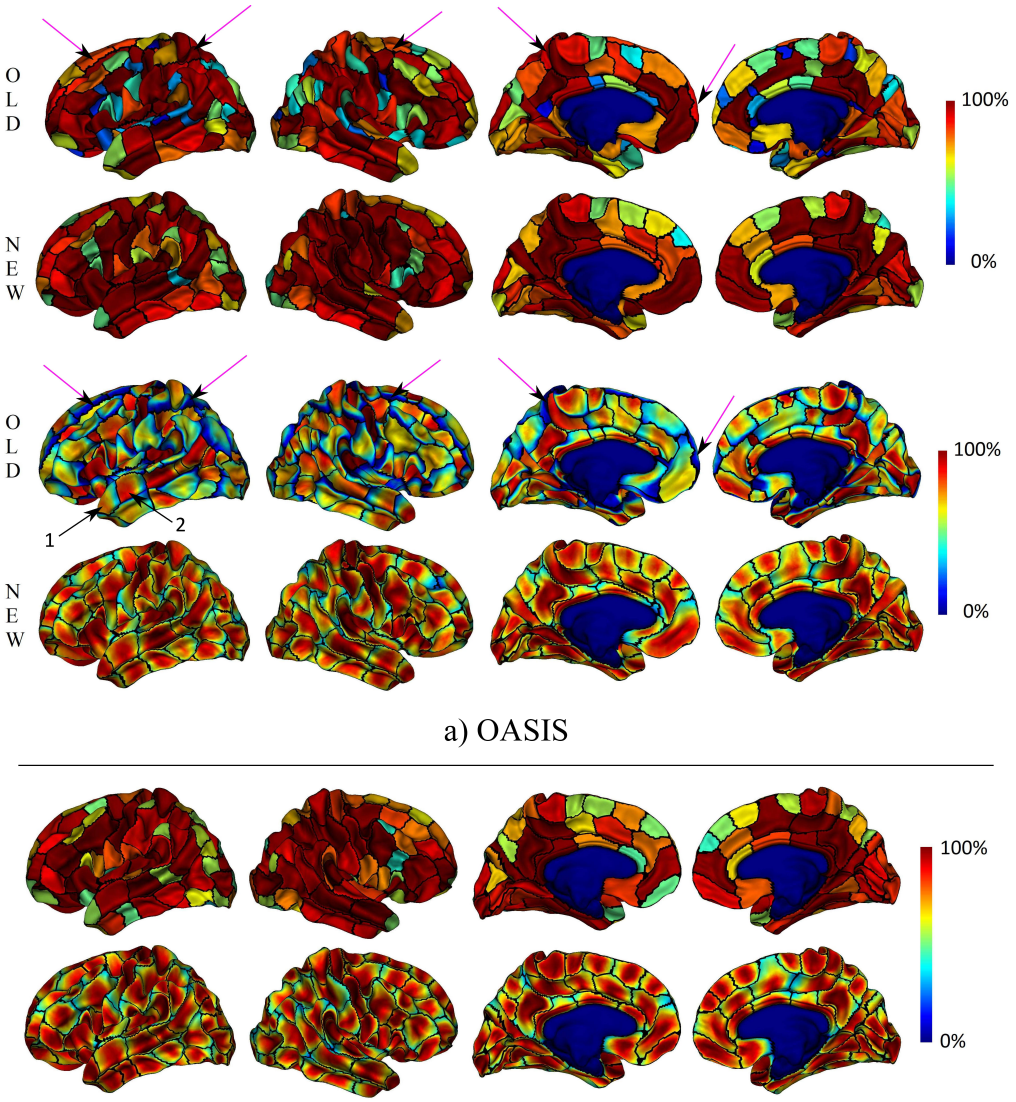

Figure 10: a) OASIS: Rows 1 & 2: Final N_1 scores, percentage of subjects that have a pit associated to a given atlas basin, after the complete pipeline. Comparison with the standard method. Rows 3 & 4: Fusion of the local influence maps. b) CMIND: Final N_1 score (first row) and fusion of the local influence maps (second row) after the complete pipeline for the right and left hemispheres.

of an exact one-to-one correspondence of basins across all subjects does not hold. This is why the output of our method is not reduced to the atlas, i.e. the average parcellation of sulcal basins, and it should not be dissociated from the frequency (N_1 score), the influence maps and the isolated pits for finer analysis. These indicators highlight which sulcal basins are robust and which are not. As an illustration, the maps displayed in Fig. 10 highlight the regions where the one-to-one correspondence assumption across subjects is coherent and where it is too strong (light blues regions, e.g. in the occipital lobes). More generally, the first two measures exhibit two types of variability:

- When the N_1 score is not maximal, it shows that some atlas basins do not exist in a part of the population.

- The influence maps show the variability in shape and location of homologous sulcal basins.

Our approach also provides the substrate for a deeper analysis of the isolated pits in future work (the pits that are not frequent enough across the population to be included in the atlas). Moreover, we integrate in the very construction of the atlas this lack of exact one-to-one correspondence: in Algorithm 1, we introduced a specific parameter for the atlas basin filtering: p corresponding to the minimal N_1 score of admissible atlas basins. This threshold defines the flexibility with respect to minor patterns of sulcal pits that we want to integrate in the atlas.

Overall, **our approach can be seen as a way to relax the need for a common unique atlas**.

5.2 Atlas: comparison

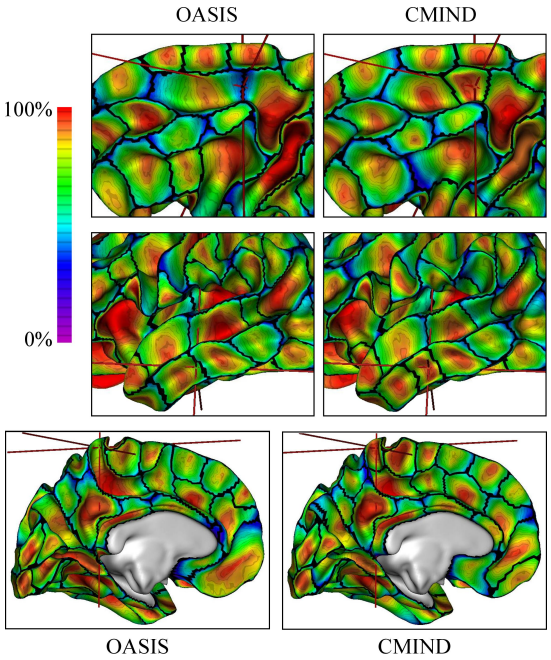

Figure 11: Atlas comparison between OASIS and CMIND. Each row highlights a region of interest where the CMIND atlas contains a basin that does not exist in the OASIS atlas.

To illustrate the input of these maps on this matter, we address hereafter the problem of atlas comparison from a methodological viewpoint. We do not intend to perform a neurological comparison between the OASIS and CMIND atlases as this goes beyond the scope of this paper. The comparison of two atlases cannot be reduced to the number of atlas basins. One should rather compare the distributions of the N_1 score than the numbers of atlas basins. The presence of atlas basins with a low N_1 scores is not robust. Indeed, they illustrate the regions where the inter-subject variability questions the existence of a single atlas. They strongly depend on the basin filtering procedure of Algorithm 1 and its stop criterion. Note that this issue is also inherent to the old pipeline (clustering on pits). For a local and fine comparison between the OASIS and CMIND atlases, we selected three regions where the CMIND atlas presents an additional atlas basin. In Fig. 11, the red cross-hair points this additional atlas basin (left column) and the corresponding area on the OASIS atlas (right column). In the examples 1 and 2 (rows 1 and 2), the N_1 scores of the additional atlas basin in CMIND are low (51% and 49%). In the first row, the large blue area, in OASIS, around the cross-hair illustrates that both density maps of the two neighboring atlas basins atlas are particularly low (40%) at their common boundary. This means that, on each side of the boundary, 60% of the identified sulcal basins do not reach this cross-hair. We can deduce

that there exists a minor pattern in the OASIS database of an additional atlas basin in this area, similar to the one in CMIND. Most likely, this minor pattern was a bit more variable in OASIS and it felt closely under the threshold value of the filtering procedure. In conclusion, the presence of this additional atlas basin in CMIND, with a low N_1, does not prove a major difference with OASIS. On the second example, the density in the OASIS atlas remains high around the cross-hair (60%). This suggests a significant difference that should be deepen. On the last example (Fig. 11, third row), the N_1 score of the additional atlas basin in CMIND is very high (78%). This high score strongly suggests an important difference with OASIS. In the OASIS atlas, the density at the location of the missing atlas basin is very high (76%). This means that 76% of the subjects in the OASIS database have a single large basin in this region that fills the top of this fold. Therefore, if we ignore the variability of sulcal basins that remains after the registration and that could partially explain the density decrease, there are at most 24% of the subjects with an additional sulcal pit around the cross-hair. This confirms an important difference between the two atlases regarding this atlas basin.

In conclusion, the density maps of sulcal basins are an efficient tool to investigate the differences between two atlases.

Remark 5.1. *Note that these two databases illustrate that sulcal pits can depend on the acquisition and preprocessing of cortical meshes. Indeed, adult subjects of the first database have about 10% less sulcal pits than the younger subjects of the second database (age range from 0 to 18). This observation is not consistent with the fact that the number of sulcal pits in this last database increases with age and this emphasizes that comprehensive analyses of sulcal pits should be based on tailored atlases of sulcal pits for any new database.*

5.3 Varifold labeling

Although Algorithm 1 provides a labeling system of the individual sulcal pits, the identification is limited to the most robust sulcal pits to improve the quality of the final atlas. Difficult labeling choices are precluded under the notion of isolated pits. Given an atlas of sulcal basins, Algorithm 2 aims at minimizing the number of such unlabeled pits. Note also that this second algorithm is independent of the atlas construction, in the sense that given a reference atlas, we can label new subjects that were not included in the atlas construction. This can be convenient for small databases whose size could question the robustness of a tailor-made atlas.

In order to evaluate the improvement of the labeling with the second part of the pipeline (the labeling with varifolds), we compared the N_1 score between the first labeling implicitly produced during the atlas construction and the final labeling. The N_1 increase is in average on both hemispheres 14.0 % for CMIND. However, this increase is not uniform and can be significantly higher in less robust basins as illustrated in Fig. 12. This figure also highlights a weakness of the geometric criterion regarding the sulcal basins whose pits are close to the boundary. In this case, the seed of the atlas basin is also close to the boundary and some individual basins that are slightly smaller than the atlas basin may not contain this seed. Although they may still significantly overlap with the atlas basin, the geometric criterion would reject them. This partially explains the important increase of sulcal basins associated to the three atlas basins with a red marker in Fig. 12.

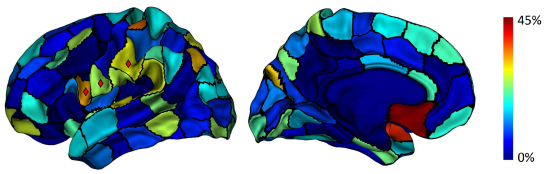

Figure 12: (CMIND) Increase of the N_1 score between the constrained labeling of the method to estimate the atlas and the optimized labeling with varifolds.

5.4 Sulcal basins define cortical parcellation

The method presented in this work produces a cortical parcellation that could be compared with the literature of brain parcellation techniques. However, we chose to present our method as a sulcal basin matching technique in order to purposely introduce the notions of inter-subjects variations and correspondences. Various approaches have been proposed for parellating the cortex in regions, introducing a great variety of constraints and modalities. See **?** for an excellent review of concepts and introduction to most common techniques. As underlined in that paper, cortical parcels refer to the concept of cortical areas that may be distinguished from its neighbors by several criteria. Since sulcal basins extraction is mainly driven by sulcal depth variations, corresponding cortical areas would be differentiated essentially from geometrical information. The relevance of such conceptualization of cortical areas deserves discussion that goes beyond the topic of the current methodological work.

6 Conclusion

In Auzias et al. (2015), authors showed that the notion of sulcal pit should not be reduced to the deepest areas of the cortical surface. This approach doubles the number of these landmarks. The resulting highly complex organization of the sulcal pits required the new methods that we presented in this paper.

The first process, presented in Section 2, builds an atlas of the sulcal organization in a group-wise parcellation of the cortical surface. This parcellation results from a derivation of the watershed by flooding algorithm where density maps of sulcal basins play the role of local depth maps and drive the segmentation. We then addressed the inter-subject labeling problem with a geometrical viewpoint and independently from the atlas problem. Besides the synergy between the two methods presented in Sections 2 and 3, the second process can be used with any given atlas allowing to label additional subjects or small databases. We successfully applied the complete pipeline to a highly heterogeneous children database. The quantitative performances were similar to those obtained on an adult database. We used the same parameters for these two very different databases which illustrated the consistency of the pipeline with respect to the characteristics of the population considered.

Besides the geometric viewpoint, a novelty of both processes is to take into account the lack of exact one-to-one correspondences between sulcal pits across subjects. On the one hand, we ensured the uniqueness of a label for each subject. On the other hand, we introduced the notion of isolated sulcal pits. These are the sulcal pits that cannot be identified by the atlas as they are not reproducible enough across the population.

Our new atlases are the first insight in the literature on the average shape of sulcal basins after registration. The density maps of sulcal basins, namely the influence maps, are a highly efficient tool to evaluate the labeling at the group level. They also seem to be a key to understand where the inter-individual variability is locally more complex. In future work, they could be used to validate and to illustrate patterns of sulcal basins in addition to the pattern analysis of sulcal pits as Meng et al. (2018) 's work.

Acknowledgments

This work was funded by the Fondation de France (Grant #2015-00059546). Data used in the preparation of this article were obtained from

- OASIS: Cross-Sectional: Principal Investigators: D. Marcus, R, Buckner, J, Csernansky J. Morris; P50 AG05681, P01 AG03991, P01 AG026276, R01 AG021910, P20 MH071616, U24 RR021382
- the C-MIND Data Repository created by the C-MIND study of Normal Brain Development. This is a multisite, longitudinal study of typically developing children from ages newborn

through young adulthood conducted by Cincinnati Children's Hospital Medical Center and UCLA and supported by the National Institute of Child Health and Human Development (Contract #s HHSN275200900018C, release 010715). A listing of the participating sites and a complete listing of the study investigators can be found at https://research.cchmc.org/c-mind. This manuscript reflects the views of the authors and may not reflect the opinions or views of the NIH.

References

Auzias, G., Brun, L., Deruelle, C., and Coulon, O. (2015). Deep sulcal landmarks: Algorithmic and conceptual improvements in the definition and extraction of sulcal pits. *Neuroimage*, 111:12–25. 2, 3, 5, 8, 9, 12, 13, 14, 15, 17, 18, 22

Brun, L., Auzias, G., Viellard, M., Villeneuve, N., Girard, N., Poinso, F., Da Fonseca, D., and Deruelle, C. (2016). Localized Misfolding Within Broca's Area as a Distinctive Feature of Autistic Disorder. *Biological Psychiatry: Cognitive Neuroscience and Neuroimaging*, 1(2):160–168. 2

Charon, N. and Trouvé, A. (2013). The Varifold Representation of Nonoriented Shapes for Diffeomorphic Registration. *SIAM Journal on Imaging Sciences*, 6(4):2547–2580. 9

Dale, A. M., Fischl, B., and Sereno, M. I. (1999). Cortical Surface-Based Analysis: I. Segmentation and Surface Reconstruction. *NeuroImage*, 9(2):179–194. 12

Fischl, B. (2012). Freesurfer. *NeuroImage*, 62(2):774–781. 12, 13

Im, K. and Grant, P. E. (2018). Sulcal pits and patterns in developing human brains. *NeuroImage*. 2

Im, K., Jo, H. J., Mangin, J.-F., Evans, A. C., Kim, S. I., and Lee, J.-M. (2010). Spatial Distribution of Deep Sulcal Landmarks and Hemispherical Asymmetry on the Cortical Surface. *Cerebral Cortex*, 20(3):602–611. 2, 3

Im, K., Raschle, N. M., Smith, S. A., Ellen Grant, P., and Gaab, N. (2016). Atypical Sulcal Pattern in Children with Developmental Dyslexia and At-Risk Kindergarteners. *Cerebral Cortex*, 26(3):1138–1148. 2

Kaltenmark, I., Brun, L., Auzias, G., Lefevre, J., Deruelle, C., and Coulon, O. (2018). Sparse description of the cortical surface pediatric development: A sulcal pits study. In *2018 IEEE 15th International Symposium on Biomedical Imaging (ISBI 2018)*, pages 990–993. 2, 3

Kaltenmark, I., Charlier, B., and Charon, N. (2017). A General Framework for Curve and Surface Comparison and Registration with Oriented Varifolds. In *2017 IEEE Conference on Computer Vision and Pattern Recognition (CVPR)*, pages 4580–4589, Honolulu, HI. IEEE. 9

Kruggel, F. (2018). The macro-structural variability of the human neocortex. *NeuroImage*, 172:620–630. 2, 17

Le Guen, Y., Auzias, G., Leroy, F., Noulhiane, M., Dehaene-Lambertz, G., Duchesnay, E., Mangin, J.-F., Coulon, O., and Frouin, V. (2018). Genetic Influence on the Sulcal Pits: On the Origin of the First Cortical Folds. *Cerebral Cortex*, 28(6):1922–1933. 2, 3

Lefèvre, J., Leroy, F., Khan, S., Dubois, J., Huppi, P. S., Baillet, S., and Mangin, J.-F. (2009). Identification of growth seeds in the neonate brain through surfacic Helmholtz decomposition. *Information Processing in Medical Imaging: Proceedings of the ... Conference*, 21:252–263. 2

Li, G., Guo, L., Nie, J., and Liu, T. (2009). Automatic cortical sulcal parcellation based on surface principal direction flow field tracking. *NeuroImage*, 46(4):923–937. 2

Lohmann, G. and von Cramon, D. Y. (2000). Automatic labelling of the human cortical surface using sulcal basins. *Medical Image Analysis*, 4(3):179–188. 2, 3

Lohmann, G., von Cramon, D. Y., and Colchester, A. C. F. (2008). Deep Sulcal Landmarks Provide an Organizing Framework for Human Cortical Folding. *Cerebral Cortex*, 18(6):1415–1420. 2

Marcus, D. S., Wang, T. H., Parker, J., Csernansky, J. G., Morris, J. C., and Buckner, R. L. (2007). Open Access Series of Imaging Studies (OASIS): Cross-sectional MRI Data in Young, Middle Aged, Nondemented, and Demented Older Adults. *Journal of Cognitive Neuroscience*, 19(9):1498–1507. 12

Meng, Y., Li, G., Lin, W., Gilmore, J. H., and Shen, D. (2014). Spatial distribution and longitudinal development of deep cortical sulcal landmarks in infants. *Neuroimage*, 100:206–218. 2

Meng, Y., Li, G., Wang, L., Lin, W., Gilmore, J. H., and Shen, D. (2018). Discovering cortical sulcal folding patterns in neonates using large-scale dataset. *Human Brain Mapping*, 39(9):3625–3635. 2, 16, 22

Régis, J., Mangin, J. F., Frouin, V., Sastre, F., Peragut, J. C., and Samson, Y. (1995). Generic Model for the Localization of the Cerebral Cortex and Preoperative Multimodal Integration in Epilepsy Surgery. *Stereotactic and Functional Neurosurgery*, 65(1-4):72–80. 2

Régis, J., Mangin, J.-F., Ochiai, T., Frouin, V., Riviére, D., Cachia, A., Tamura, M., and Samson, Y. (2005). "Sulcal Root" Generic Model: a Hypothesis to Overcome the Variability of the Human Cortex Folding Patterns. *Neurologia medico-chirurgica*, 45(1):1–17. 2

Rettmann, M. E., Han, X., Xu, C., and Prince, J. L. (2002). Automated Sulcal Segmentation Using Watersheds on the Cortical Surface. *NeuroImage*, 15(2):329–344. 3

Takerkart, S., Auzias, G., Brun, L., and Coulon, O. (2017). Structural graph-based morphometry: A multiscale searchlight framework based on sulcal pits. *Medical image analysis*, 35:32–45. 2

Yang, F. and Kruggel, F. (2008). Automatic segmentation of human brain sulci. *Medical image analysis*, 12(4):442–451. 2